

A Stretchable Electronic Fabric Artificial Skin with Pressure-, Lateral Strain-, and Flexion-Sensitive Properties

Jin Ge, Li Sun, Fu-Rui Zhang, Ye Zhang, Lu-An Shi, Hao-Yu Zhao, Hong-Wu Zhu, Hai-Long Jiang, and Shu-Hong Yu*

Human skin with a network of highly sensitive sensory receptors is able to transmit various mechanical stimuli from external environment to the brain.^[1] Interest in realizing this function in an artificial skin is motivated by the promise of creating advanced humanoid robots, biomedical prostheses, surgical electronic gloves, and wearable health monitoring devices.^[2] To mimic the properties of human skin, artificial skin should have the ability of measuring the spatial distribution of the stress induced by multiple mechanical stimuli such as normal pressure, lateral strain, and flexion, as it allows object manipulation, grasp control, and recording of body movement.^[1b,c] Second, stretchability is an important property for artificial skins, ensuring they conformably cover arbitrary curved and moving surfaces such as joints of the robot's arm, and withstand repeated and prolonged mechanical deformation such as bending and twisting.^[3] Third, to realize the wide application of artificial skin in our daily lives, the artificial skin should be compatible with large-area implementation and low materials and fabrication cost.^[1c,2k,3a,4]

In the past decade, the development of artificial skin based on pressure sensors arrays on flexible substrate has achieved great progresses, reporting increasing sensitivity, response speed, and resolution of tactile mapping.^[2b,c,f,g,k,4,5] But unlike human skin, these pressure sensor arrays lacked stretchability and were limited to the function of providing information of spatial pressure distribution. To solve these problems, the choosing of intrinsically stretchable materials and new architecture design of mechanical sensors are effective strategies to fabricate stretchable mechanical sensors with multiple mechanical force sensitivities.^[6] For example, Suh and co-workers^[2l] developed a skin-attachable strain-gauge sensor based on nanoscale mechanical interlocking between metal-coated nanofibers, the reversible interlocking of these conductive nanofibers enable the detection of pressure, shear, and torsion. Bao and

co-workers provided a stretchable mechanical sensor capable of sensing pressure, lateral strain, and flexion by sandwiching a porous rubber layer and air gap between two stretchable carbon nanotube film electrodes.^[6e] Although multiple mechanical force sensitivities have been achieved for single sensor unit, a corresponding sensor array with stretchable and multiple force mapping properties has not been demonstrated. The primary challenge of fabricating stretchable sensor array devices with multiple force mapping properties is not only to ensure the simultaneous achievement of excellent mechanical robustness and sensing performance for the sensor elements but also to achieve high mechanical adhesion as well as good electronic contact between elastic conducting wiring and sensor elements.^[7] Recently, based on the geometric structuring strategy, a stretchable artificial skin with multiple force mapping properties has been reported by Kim and co-workers,^[1b] in which various sensing elements were integrated on a stretchable serpentine silicon nanoribbon networks. Despite the high performance obtained, the large area fabrication of this highly integrated artificial skin based on silicon nanoribbon is complicated and expensive, which would hinder its practical and wide application.

Here, we report a low-cost electronic fabric with stretchable sensor arrays which can simultaneously map and quantify the mechanical stresses induced by normal pressure, lateral strain, and flexion. The fabric is based on intertwined composite fibers (named as sensor electrodes) with piezoresistive rubber as the shell sensing element and helical silver nanowires network as the stretchable and highly conductive core electrode. Mechanical sensor unit forms at each cross contact between the sensor electrodes. The coaxial structure of the stretchable sensor electrode and fibrous architecture of the sensor unit are the key points for the fabric sensor arrays to allow stretching at the system level and to realize multiple force sensitivities. This electric fabric exhibits excellent performance under stretched state and prolonged usage. The pressure sensitivity of the sensor unit can keep more than 50% of its original value even the tensile strain of sensor electrodes increases up to 100%. The sensing response of the sensor unit to pressure is highly repeatable and reproducible up to 100 000 cycles with excellent on/off switching behavior. We anticipate that this low-cost electronic fabric has potential applications in artificial skin for humanoid robotics, biomedical prostheses, and physiological analysis devices.

The fabrication processes of the electronic fabric are illustrated in **Figure 1a**. A commercial elastic thread with inner polyurethane fibers as the core and nylon fiber helically wound around their surfaces (**Figure S1**, Supporting Information) was

J. Ge, L. Sun, F.-R. Zhang, Y. Zhang,
L.-A. Shi, H.-Y. Zhao, H.-W. Zhu,
Prof. H.-L. Jiang, Prof. S.-H. Yu
Division of Nanomaterials and Chemistry
Hefei National Laboratory for Physical
Sciences at Microscale
Collaborative Innovation Center of
Suzhou Nano Science and Technology
Department of Chemistry, Hefei Science Center, CAS
University of Science and Technology of China
Anhui 230026, P. R. China
E-mail: shyu@ustc.edu.cn



DOI: 10.1002/adma.201504239

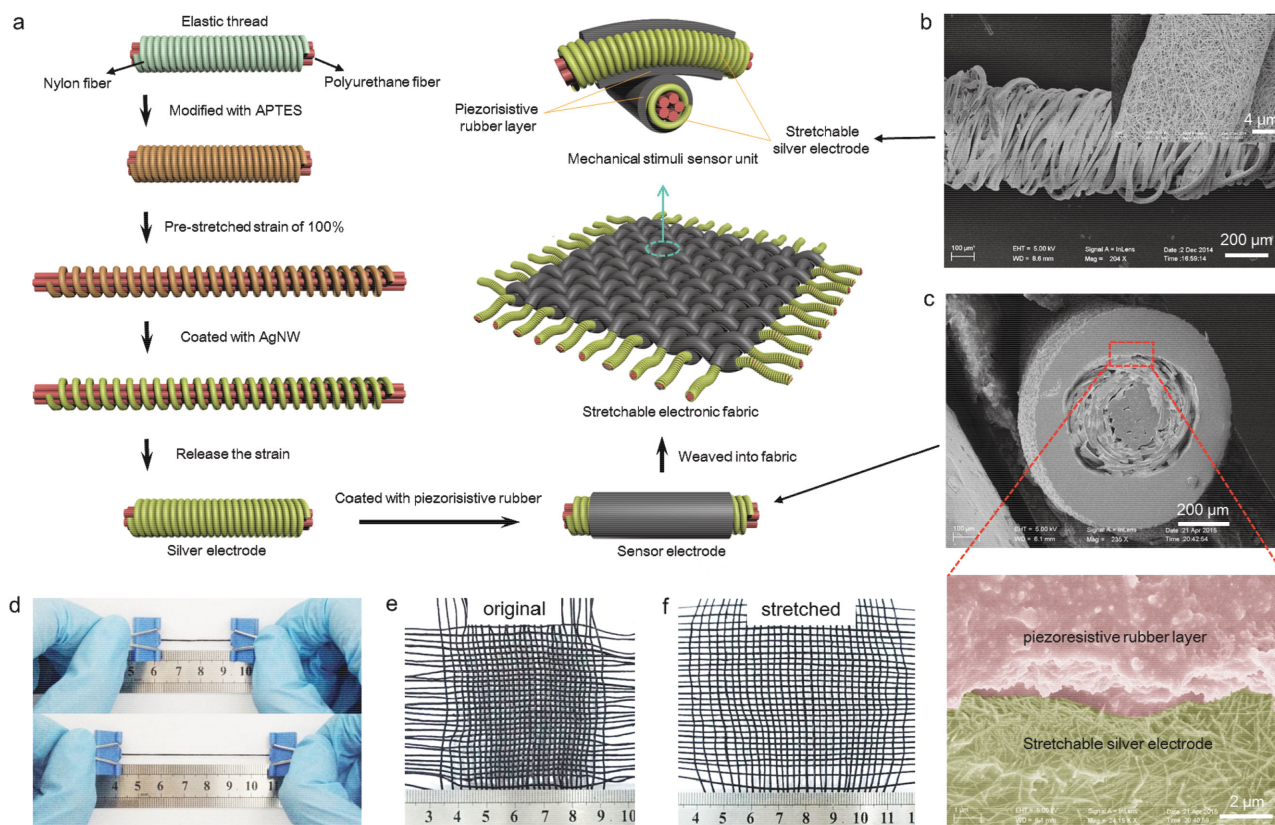


Figure 1. Fabrication of the electronic fabric. a) Schematic illustration of the fabrication processes of the electronic fabric with fibrous sensor units. b) SEM images of the silver electrode. c) SEM images of the cross section of the sensor electrode. d) Optical images of the original and stretched sensor electrode. e, f) Optical images of the electronic fabric and that under biaxial stretched state.

first treated with 3-triethoxysilylpropylamine (APTES) in order to form a hydrogen bond between -NH_2 of APTES and $>\text{C}=\text{O}$ of polyvinyl pyrrolidone on the AgNWs (Figure S2, Supporting Information). Then the modified elastic thread was stretched to 100% of tensile strain and coated with AgNW dispersion through a facile dip-coating process. The prestretch operation is aimed to make the nylon fibers detached from each other and facilitate the coating of AgNWs on the inner surface of nylon fibers, which is important to form helical AgNWs network and achieve highly stable electronic conductivity under tensile deformation (Figure S3, Supporting Information). After releasing the strain, a stretchable and highly conductive electrode based on helical AgNWs networks was obtained (hereafter noted as silver electrode). Then, a kind of stretchable and piezoresistive rubber,^[8] which was composed of polydimethylsiloxane (PDMS) and carbon black, was chosen as the force sensing element to coat the surface of the silver electrode through a dip-coating processes. The obtained composite fibers (hereafter noted as sensor electrodes) could be easily weaved into large area fabric, in which mechanical sensor units formed at each cross contact.

Figure 1b shows a typical scanning electron microscopy (SEM) image of the silver electrode. The AgNWs are homogeneously immobilized on the surface of nylon fibers, forming helical AgNWs networks. Due to this unique helical structure, the AgNWs networks can withstand large tensile strain without reducing the conductive paths between silver nanowires and as

a result keep high conductivity (Figure S4, Supporting Information). Figure 1c shows the SEM images of the cross section of a sensor electrode, which exhibit the coaxial structure and the close contacted interface between AgNWs coating and the piezoresistive rubber layer. This unique coaxial structure endows the sensor electrode with close connection between silver electrode and the conductive rubber under mechanical deformation, which is highly important for the sensor unit to output stable and reversible electric signals. Figure 1d shows that the sensor electrode can be stretched to 100% of tensile strain as that of the elastic thread and silver electrode. The sensor electrodes can be readily intertwined to large area electronic fabric. Figure 1e shows a typical electronic fabric, in which each cross contact forms a sensor unit. Due to the stretchability of the sensor electrodes, the fabric sensor arrays is stretchable (Figure 1f) and can be applied on arbitrary curved and moving surfaces.

To study the sensing mechanism of the sensor unit, two sensor electrodes were stacked perpendicularly to each other (Figure 2a), then a piezoresistive mechanical sensor formed at the cross contact point between the sensor electrodes. Figure 2b illustrates that the resistance between two silver electrodes comprises of contact resistance which is depend on the contact area (A) between the sensor electrodes and the materials resistance of the piezoresistive rubber layer which is influenced by the conductivity and thickness (d) of the piezoresistive rubber. Therefore, when a mechanical force is applied on the sensor unit, the

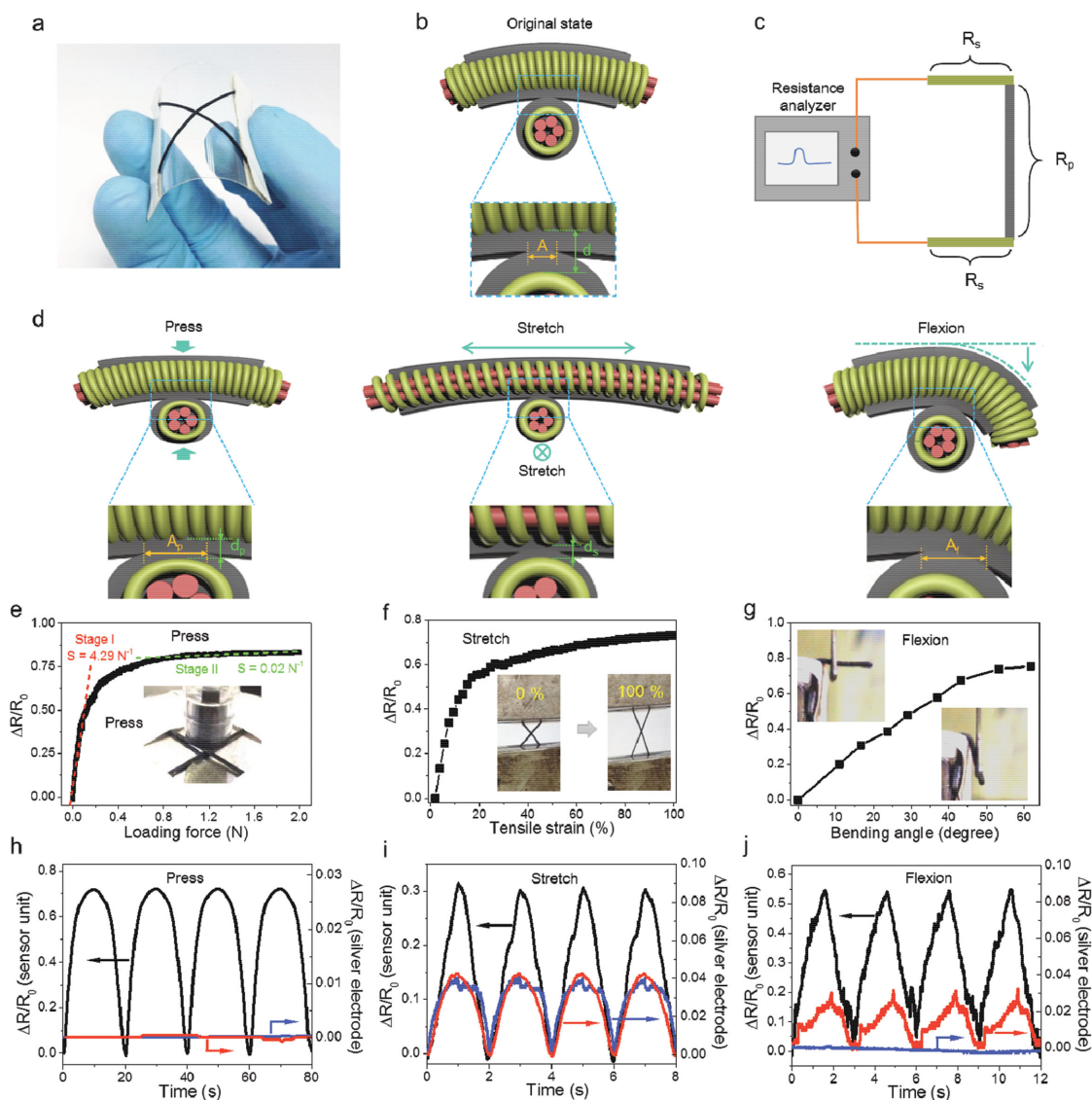


Figure 2. Mechanical–electric properties of the sensor unit. a) Optical image of a typical sensor unit on a flexible polyethylene terephthalate (PET) substrate. b) Schematic illustration of the cross contact point of the sensor unit. A is the contact area and d is the thickness of the piezoresistive rubber layers between the silver electrodes. c) The equivalent circuit of the sensor unit. R_s is the resistance of silver electrode ($\approx 0.5 \Omega \text{ cm}^{-1}$). R_p is the resistance of the piezoresistive rubber between the silver electrodes at the cross contact area ($\approx 500 \Omega$). d) Schematic illustration of the shape deformation at the contact point of the sensor unit under press, stretch, and flexion. A_p and d_p are the contact area and thickness under press, d_s is the thickness under stretch, and A_f is the contact area under flexion. e–g) The plots of relative resistance change ($\Delta R/R_0$) of the sensor unit as a function of loading force, tensile strain, and bending angle respectively. h–j) Relative resistance change of the sensor unit (black curves), silver electrodes (blue and red curves) as a function of time at incrementally increasing and decreasing loading force (0–0.35 N), tensile strain (0%–8%), bending angle (0° – 35°), respectively. Detailed test methods are illustrated in Figure S9 (Supporting Information).

change of contact area, thickness, and conductivity of the piezoresistive rubber will result in electric signals of resistance change. In order to measure this resistance change, the silver electrodes of the sensor unit were connected to a resistance analyzer (Keithley 4200 SCS), and the whole resistance of the sensor unit was obtained. The sensitivity of the sensor unit is subject to the value of relative whole resistance change ($(R_0 - R)/R_0$), R_0 and R is the whole resistance before and after applying a mechanical force on the sensor unit. The equivalent circuit is illustrated in Figure 2c. The whole resistance comprises of the resistance of silver electrodes (R_s) and the resistance of piezoresistive rubber

(R_p). Therefore, the relative resistance change can be expressed as $(R_0 - R)/R_0 = (R_{s0} - R_s + R_{p0} - R_p)/(R_{s0} + R_{p0})$, where R_{s0} and R_{p0} are the original resistance of silver electrodes and piezoresistive rubber, respectively. Because of the high conductive and stability of silver electrodes discussed above, R_{s0} ($\approx 0.5 \Omega \text{ cm}^{-1}$) is far smaller than R_{p0} ($\approx 500 \Omega$), and the resistance change of the silver electrodes ($R_{s0} - R_s$) is very small. Therefore, the whole resistance change ($(R_0 - R)/R_0$) can be further approximated as $(R_{p0} - R_p)/R_{p0}$, which means the sensitivity of the sensor unit mainly depends on the relative resistance change of piezoresistive rubber layers between the two silver electrodes.

Figure 2d illustrates the shape deformation of the sensor unit at the cross contact point under mechanical stimuli of press, stretch, and flexion. Because of that all these kinds of forces can change the contact area (A in Figure 2b) between the two silver electrodes and/or thickness (d in Figure 2b) of the conductive rubber, the fibrous sensor unit has multiple sensing properties. To estimate the pressure sensitivity of the sensor unit, the relative whole resistance change ($\Delta R/R_0$) of the sensor unit was calculated on the basis of measured values and potted as the function of applied loading force (F) as shown in Figure 2e. The pressure sensitivity S can be defined as the slope of the curve in Figure 2e ($S = \delta(\Delta R/R_0)/\delta F$). It can be seen that the sensitivity ($S = 4.29 \text{ N}^{-1}$) of the sensor unit in the low loading force range (named as stage I) is far higher than that ($S = 0.02 \text{ N}^{-1}$) in the high loading force range (named as stage II). This big difference of sensitivities is due to the different sensing mechanisms in the two stages (Figure S5, Supporting Information). At the stage I, a small loading force can change the physical appearance of the sensor electrode from round shape to tabular shape, resulting in the increase of the contact area between the conductive rubber layers, which greatly decrease the resistance between the silver electrodes. At the stage II, the decrease of resistance between the silver electrodes is mainly caused by the conductivity increase of the piezoresistive rubber layers, which requires large loading force to close the carbon black particles in the rubber matrix. Therefore, this fibrous sensor structure can increase the pressure sensitivity of traditional conductive rubber materials. The sensor unit is also sensitive to stretch based on the thickness decrease of conductive rubber layer (d_c) under tensile strain (Figure 2d). To measure the resistance change of the sensor unit under stretch, two sensor electrodes was stacked perpendicularly to each other and two sides the sensor electrodes were fixed by clamps respectively (Figure S6, Supporting Information). Then the clamp was rotated by 45° of angle to simulate the state of sensor electrodes weaved in a fabric. The resistance of the sensor unit was recorded during the tensile strain. The resistance change ($\Delta R/R_0$) was calculated and plotted as a function of tensile strain. As can be seen in Figure 2f, the resistance change increases quickly with the tensile strain until 20%, then increases slowly with the tensile strain. The reason may be that the conductivity of the conductive rubber layer decreased quickly under tensile strain above 20% of tensile strain, which partially compensated the resistance decrease caused by the thickness decrease of the conductive rubber layer. To study the effect of flexion on the resistance change of the sensor unit, two perpendicularly stacked sensor electrodes were immobilized on a hard substrate with half part of one sensor electrode hanging in the air (Figure S7, Supporting Information). Then a "Y" type fork was used to bend the hanged electrode and the resistance of the sensor unit was recorded. Figure 2g shows the curve of resistance change ($\Delta R/R_0$) versus bending angle of the hanged electrode. It can be seen that the resistance change increased almost linearly with the increase of bending angle, which is in accordance with the contact sensing mode illustrated in Figure 2d. In this mode, the contact area (A_f) between the sensor electrodes increases linearly with the increase in bending angle. To demonstrate the high durability of the sensor unit, cycle tests were performed. The signal of resistance change kept stable and reversible even

after 100 000 times of press-release cycles (Figure S8, Supporting Information).

The ability to distinguish different kinds of input mechanical stimuli is also important for electronic skin, which remains a challenge.^[1c,6e] Here, the above-mentioned three kinds of mechanical stimuli may be distinguished by the sensor unit itself based on the different behavior of silver electrodes under press, stretch, and flexion. To verify this assumption, the resistance change of the sensor unit along with silver electrodes was simultaneously measured during the mechanical deformation processes (Figure S9, Supporting Information). Figure 2h shows that the relative resistance change of the sensor unit increased with the vertical loading force, while negligible changes in the resistance of the two silver electrodes were observed due to the lack of lateral straining of the silver electrodes. When the sensor unit was stretched, both two silver electrodes were elongated under the same tensile strain, and as a result the resistances of both two silver electrodes increased with the tensile strain under the same change rate (Figure 2i). Under flexion, the tensile stress only appeared on the bended sensor electrode, and only the resistance of bended sensor electrode increased with the bending angle while the resistance of the other sensor electrode experienced negligible change (Figure 2j). Therefore, based on the different resistance responses of the silver electrodes to press, stretch, and flexion, our sensor unit has the ability of distinguishing a variety of mechanical stimuli.

Beside the ability of covering on deformable surfaces, stretchable sensors should keep their force sensitivity under stretched state. To study the pressure sensitivity of the sensor unit under the stretched state, the sensor electrodes were stretched to a certain tensile strain, then the mechanical–electrical test was performed. Figure 3a shows the plots of resistance change of the sensor units under different tensile strain as a function of loading force. It can be seen that the resistance change of all the stretched sensor units increase with the applied loading force as that of the original sensor unit. Corresponding sensitivities ($S = \delta(\Delta R/R_0)/\delta F$) at stage I decrease to 68.4%, 53.4%, 87.3%, at 30%, 50%, and 100% of tensile strain, respectively, and the sensitivities at stage II almost keep the same value as that of the original value (Figure S10, Supporting Information). Therefore the sensor unit can be applied on arbitrary curved and moving surface and keep more than 50% of its original pressure sensitivity. Although various stretchable pressure sensors with multiple force sensing properties have been reported,^[6e,f,9] their pressure sensing performance under stretched state were not demonstrated.

To shed light on the response speed of the sensor unit, time-resolved measurement was performed. External pressure with a frequency of up to 60 Hz was applied on the sensor unit while measuring the resistance change. Figure 3b shows that the profile of the output electrical signal is regular and repeatable even when the frequency of pressure increases to 60 Hz. The time-resolved resistance signal of one pressure cycle exhibits that the response speed of the sensor unit to outside pressure could reach to 8 ms (Figure 3c). In addition, the sensor unit also exhibited little hysteresis to input pressure force. Only 5 ms of delay time were detected for a frequency of ≈ 5 Hz (Figure S11a,b, Supporting Information). This low hysteresis time is due to that the resistance change of the sensor unit

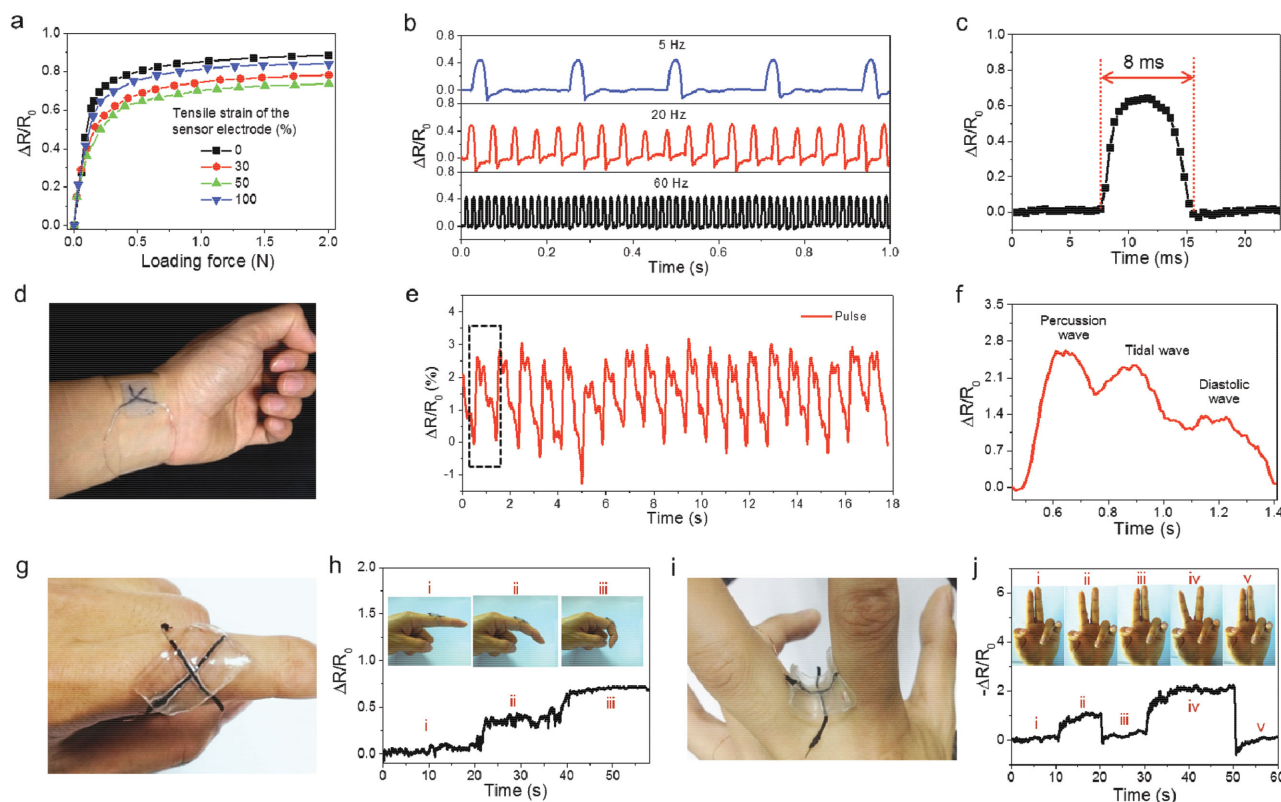


Figure 3. Applications of the fibrous sensor unit. a) The plots of the resistance change of the sensor units under various tensile strain as a function of the loading force. b) Response of the sensor unit to input pressure with various frequencies (5, 20, and 60 Hz) as a function of time. c) A typical resistance change–time plot for the pressure of 60 Hz in (b). d) Optical image of the sensor unit device placed on the artery of a human wrist. e) Resistance change–time plot for the sensor unit mounted on the wrist (≈ 67 beats per minute). f) Resistance change–time plot for data in the region indicated by the dashed box in (e). g) Optical image of a sensor unit mounted on the joint of a finger. h) Resistance change–time plot for the sensor in (g), insets are the photographs of finger motion. i) Optical image of a sensor unit device mounted on the web between fingers. j) Resistance change–time plot for the sensor in (i), insets are the photographs of finger configurations.

is based on the shape deformation of the sensor electrode with round shape and rough surface (Figure S11c,d, Supporting Information) rather than traditional flat electrode.^[5a] The fast sensing performance of the sensor unit to pressure is very helpful to detect force variation such as human pulse wave in real time. Figure 3d shows that a sensor unit, which was switched between two pieces of silicon rubber mat, was fixed on an adult human wrist by scotch tape. The resistance change was measured by a resistance analyzer (Keithley 4200 SCS) with high response time. Figure 3e shows the real-time record over 20 pulse periods in 18 s, indicating the heartbeat of 67 times per minute. In addition, due to the fast sensing response of the sensor unit, a characteristic pulse pressure shape with three clearly distinguishable peaks containing percussion wave, tidal wave, and diastolic wave were obtained (Figure 3f). These peaks reveal some physiological signals of human body such as systolic, diastolic blood pressure, and the heart rate, which can be used for disease diagnosis.^[10] It should be noted that the majority of the sensors used in arterial tonometry cannot detect the diastolic tail. Therefore our sensor unit has potential applications in more detailed diagnostics.^[5b]

The strain and flexion sensing properties of the sensor unit also have potential application in monitoring the posture and movement of human body. To attach the sensor unit on

human skin comfortably, two pieces of stretchable acrylic elastomer (3M VHB 4910) were used to sandwich the sensor unit. Figure 3g shows a sensor unit mounted on the joint of a human finger. The resistance change was recorded in real time during the bending processes of the finger. Figure 3h shows that the resistance change increases with the bending angle of human finger. Based on the measured value of the electrical signals, the finger configuration can be assessed. When the sensor unit was fixed on the finger web (Figure 3i), the finger posture such as opening and closing could be monitored. Figure 3j shows that the opening angle of the fingers can be detected from the absolute value of resistance change. Due to the multiple sensing properties of the sensor unit, the posture and moving of the whole body could be fully recorded by mounting the sensor units on each joint of the human or robot body.

Detecting the position of mechanical stimuli, which needs a matrix of force sensors, is an important function of artificial skin devices. To demonstrate the force mapping properties of the electronic fabric, a proof-of-concept electronic fabric (4 cm \times 4 cm) with 10 pixel \times 10 pixel sensor units array was fabricated (Figure 4a). The electronic fabric was adhered to a stretchable silicon rubber mat to avoid affecting the pixels in the immediate vicinity of the loading force and therefore reduced the cross talk between adjacent pixels (Figure S12, Supporting Information).

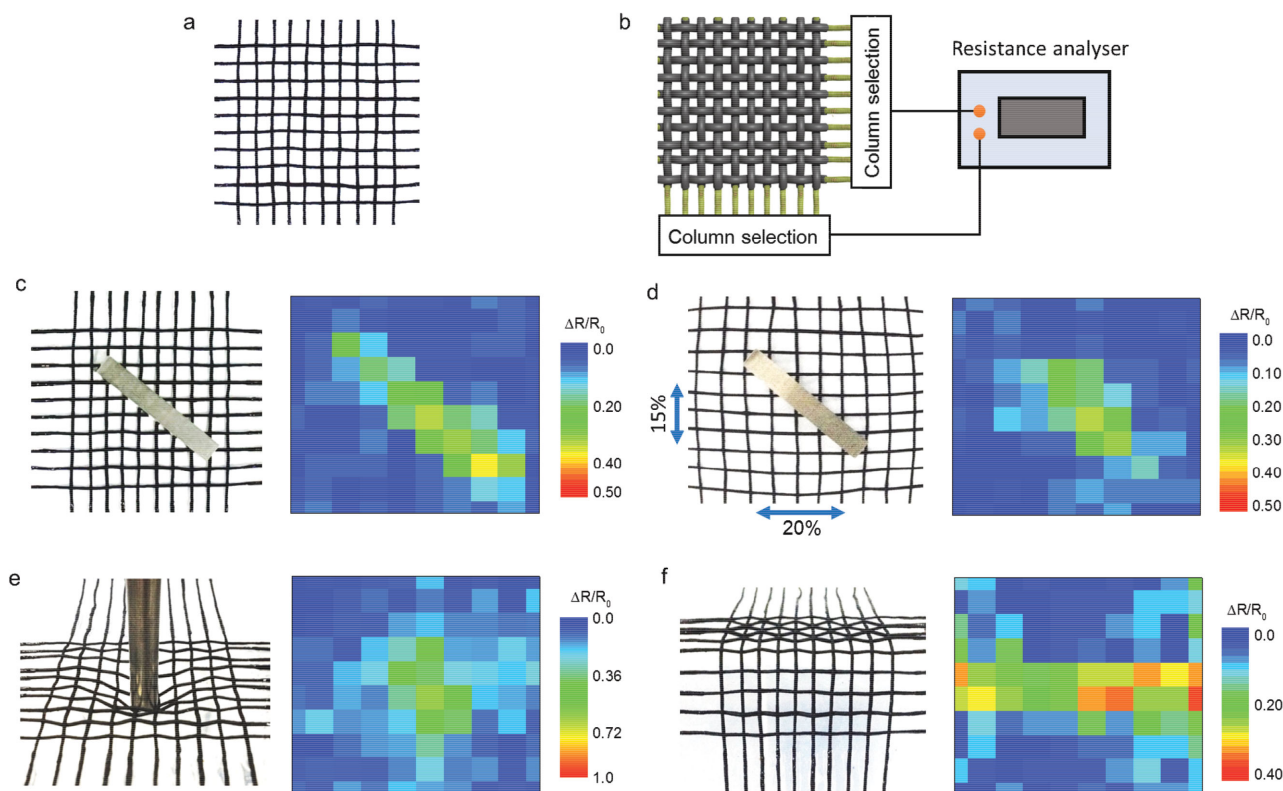


Figure 4. Force mapping properties of the electronic fabric. a) Photograph of an electronic fabric (4 cm × 4 cm) with sensor units array of 10 pixels × 10 pixels. b) Schematic of the measurement method. The resistances of each sensor unit can be measured (Figure S13, Supporting Information). c) Photograph of an electronic fabric with an iron cuboid placed on the top for applying pressure (left) and corresponding 2D intensity profile obtained from experimental mapping of the sensor unit signals (right). d) Photograph of the stretched electronic fabric (15% strain at column direction and 20% strain at row direction) with an iron cuboid placed on the top for applying pressure (left) and corresponding 2D intensity profile of resistance changes for each sensor unit. e) Photograph of an electronic fabric with an iron rod poking its surface (left) and corresponding 2D intensity profile of resistance changes for each sensor unit. f) Photograph of an electronic fabric under bending state (left) and corresponding 2D intensity profile of resistance changes for each sensor unit.

The resistance between each row and vertical silver electrodes is measured before and after the loading of mechanical force (Figure 4b). Mapping out the absolute resistance changes ($|\Delta R/R_0|$) will clearly exhibit the 2D forcing distribution on the electronic fabric (Figure S13, Supporting Information). To study the pressure mapping function of the electronic fabric, a metal cuboid with an area of $3.35 \times 0.52 \text{ cm}^2$ was placed on the top of the sensor unit array, followed by application a normal pressure of $\approx 7.2 \text{ kPa}$. Figure 4c shows that the applied pressure profile was spatially resolved by the electronic fabric. To further demonstrate the pressure mapping properties of the electronic fabric under mechanical deformation, the electronic fabric was stretched biaxially with 20% at row direction and 15% at column direction, then the same pressure mapping test was performed as above. Figure 4d shows that applied pressure profile can also be mapped, which indicates that the electronic fabric can keep its pressure mapping function when it is immobilized on an arbitrary curved and moving surfaces.

Besides having the ability to sense normal vertical pressure, human skin can also feel a range of flexion and lateral strain at different body locations, which suggests the need for mechanical sensors that can detect lateral strain and flexion for artificial skins to characterize the mechanical behavior of body

movements and skin mechanics.^[1b] To study the lateral strain mapping properties of the electronic fabric, two opposite sides of the electronic fabric were fixed by two clamps and a glass tube was placed behind it as a support, followed by placing an iron rod (170 g of weight) on the electronic fabric (Figure S14, Supporting Information). As shown in Figure 4e, the iron rod induced large tensile strains around its head on the electronic fabric. The resistance changes data were gathered and plotted into 2D map. The color contrast mapping clearly shows that the value of strain force closely around the iron rod is bigger than that on the side position of the electronic fabric, which is highly consistent with the shape deformation of the electronic fabric, demonstrating the exact response of our obtained electronic fabric to lateral strain. To further study the flexion mapping property of the electronic fabric, a bendable substrate based on two plastic plates jointed together by scotch tape was used to support the electronic fabric (Figure S15, Supporting Information). Bending the substrate only induces the flexion of electronic fabric at the joint position and other region was not affected. Figure 4f shows the electronic fabric under bending state and the corresponding 2D map of resistance change. The color contrast map clearly shows that the spatial distribution of the stress was mainly focused on the flexion region of the

electronic fabric, which demonstrated that the electronic fabric has the ability of mapping out the region of flexion.

In summary, we provide an electronic fabric based on intertwined sensor electrodes with piezoresistive rubber as the shell sensing element and silver nanowires coated elastic thread as the stretchable and highly conductive core electrode. The unique coaxial structure of the stretchable sensor electrode and fibrous sensor architecture avoid the disconnection between stretchable conductors and sensor units under mechanical deformation, which made the resulted fabric sensor arrays not only stretchable at system level but also have multiple force mapping properties. We demonstrated that the electronic fabric has the ability of simultaneously mapping and quantifying the mechanical stresses induced by pressure, lateral strain, and flexion. We also proved that the sensor unit can be used to detect the detailed diagnostic information of human pulse wave and to record the body posture and movement. We envision that this stretchable electronic fabric with multiple force mapping properties and high durability has potential applications in wearable artificial skin for humanoid robotics, biomedical prostheses, and physiological analysis devices.

Supporting Information

Supporting Information is available from the Wiley Online Library or from the author.

Acknowledgements

This work was supported by the National Natural Science Foundation of China (Grant Nos. 21431006 and 91227103), the Foundation for Innovative Research Groups of the National Natural Science Foundation of China (Grant No. 21521001), the National Basic Research Program of China (Grant Nos. 2014CB931800 and 2013CB933900), the Users with Excellence and Scientific Research Grant of Hefei Science Center of Chinese Academy of Sciences (Grant Nos. 2015HSC-UE007, 2015SRG-HSC038).

Received: August 30, 2015

Revised: October 8, 2015

Published online: November 30, 2015

- [1] a) A. Zimmerman, L. Bai, D. D. Ginty, *Science* **2014**, *346*, 950; b) J. Kim, M. Lee, H. J. Shim, R. Ghaffari, H. R. Cho, D. Son, Y. H. Jung, M. Soh, C. Choi, S. Jung, K. Chu, D. Jeon, S. T. Lee, J. H. Kim, S. H. Choi, T. Hyeon, D. H. Kim, *Nat. Commun.* **2014**, *5*, 5747; c) M. L. Hammock, A. Chortos, B. C. K. Tee, J. B. H. Tok, Z. A. Bao, *Adv. Mater.* **2013**, *25*, 5997.
- [2] a) S. Xu, Y. Zhang, L. Jia, K. E. Mathewson, K. I. Jang, J. Kim, H. Fu, X. Huang, P. Chava, R. Wang, S. Bhole, L. Wang, Y. J. Na, Y. Guan, M. Flavin, Z. Han, Y. Huang, J. A. Rogers, *Science* **2014**, *344*, 70; b) W. Wu, X. Wen, Z. L. Wang, *Science* **2013**, *340*, 952; c) V. Maheshwari, R. F. Saraf, *Science* **2006**, *312*, 1501; d) Z. Q. Ma, *Science* **2011**, *333*, 830; e) D. H. Kim, N. S. Lu, R. Ma, Y. S. Kim, R. H. Kim, S. D. Wang, J. Wu, S. M. Won, H. Tao, A. Islam, K. J. Yu, T. I. Kim, R. Chowdhury, M. Ying, L. Z. Xu, M. Li, H. J. Chung, H. Keum, M. McCormick, P. Liu, Y. W. Zhang, F. G. Omenetto, Y. G. Huang, T. Coleman, J. A. Rogers, *Science* **2011**, *333*, 838; f) S. Gong, W. Schwalb, Y. W. Wang, Y. Chen, Y. Tang, J. Si, B. Shirinzadeh, W. L. Cheng, *Nat. Commun.* **2014**, *5*, 3132; g) D. Kang, P. V. Pikhitsa, Y. W. Choi, C. Lee, S. S. Shin, L. Piao, B. Park, K. Y. Suh, T. I. Kim, M. Choi, *Nature* **2014**, *516*, 222; h) M. Kaltenbrunner, T. Sekitani, J. Reeder, T. Yokota, K. Kuribara, T. Tokuhara, M. Drack, R. Schwodiauer, I. Graz, S. Bauer-Gogonea, S. Bauer, T. Someya, *Nature* **2013**, *499*, 458; i) B. C. Tee, C. Wang, R. Allen, Z. Bao, *Nat. Nanotechnol.* **2012**, *7*, 825; j) D. Son, J. Lee, S. Qiao, R. Ghaffari, J. Kim, J. E. Lee, C. Song, S. J. Kim, D. J. Lee, S. W. Jun, S. Yang, M. Park, J. Shin, K. Do, M. Lee, K. Kang, C. S. Hwang, N. Lu, T. Hyeon, D. H. Kim, *Nat. Nanotechnol.* **2014**, *9*, 397; k) K. Takei, T. Takahashi, J. C. Ho, H. Ko, A. G. Gillies, P. W. Leu, R. S. Fearing, A. Javey, *Nat. Mater.* **2010**, *9*, 821; l) C. Pang, G. Y. Lee, T. I. Kim, S. M. Kim, H. N. Kim, S. H. Ahn, K. Y. Suh, *Nat. Mater.* **2012**, *11*, 795.
- [3] a) T. Someya, Y. Kato, T. Sekitani, S. Iba, Y. Noguchi, Y. Murase, H. Kawaguchi, T. Sakurai, *Proc. Natl. Acad. Sci. USA* **2005**, *102*, 12321; b) T. Sekitani, Y. Noguchi, K. Hata, T. Fukushima, T. Aida, T. Someya, *Science* **2008**, *321*, 1468; c) D.-H. Kim, N. Lu, R. Ma, Y.-S. Kim, R.-H. Kim, S. Wang, J. Wu, S. M. Won, H. Tao, A. Islam, K. J. Yu, T.-I. Kim, R. Chowdhury, M. Ying, L. Xu, M. Li, H.-J. Chung, H. Keum, M. McCormick, P. Liu, Y.-W. Zhang, F. G. Omenetto, Y. Huang, T. Coleman, J. A. Rogers, *Science* **2011**, *333*, 838; d) M. Park, J. Park, U. Jeong, *Nano Today* **2014**, *9*, 244.
- [4] T. Someya, T. Sekitani, S. Iba, Y. Kato, H. Kawaguchi, T. Sakurai, *Proc. Natl. Acad. Sci. USA* **2004**, *101*, 9966.
- [5] a) S. C. B. Mannsfeld, B. C. K. Tee, R. M. Stoltenberg, C. V. H. H. Chen, S. Barman, B. V. O. Muir, A. N. Sokolov, C. Reese, Z. Bao, *Nat. Mater.* **2010**, *9*, 859; b) G. Schwartz, B. C. K. Tee, J. G. Mei, A. L. Appleton, D. H. Kim, H. L. Wang, Z. N. Bao, *Nat. Commun.* **2013**, *4*, 1859; c) L. J. Pan, A. Chortos, G. H. Yu, Y. Q. Wang, S. Isaacson, R. Allen, Y. Shi, R. Dauskardt, Z. N. Bao, *Nat. Commun.* **2014**, *5*, 3002; d) C. Y. Hou, H. Z. Wang, Q. H. Zhang, Y. G. Li, M. F. Zhu, *Adv. Mater.* **2014**, *26*, 5018.
- [6] a) C. Yan, J. Wang, W. Kang, M. Cui, X. Wang, C. Y. Foo, K. J. Chee, P. S. Lee, *Adv. Mater.* **2014**, *26*, 2022; b) L. Viry, A. Levi, M. Totaro, A. Mondini, V. Mattoli, B. Mazzolai, L. Beccai, *Adv. Mater.* **2014**, *26*, 2659; c) M. Ramuz, B. C. K. Tee, J. B. H. Tok, Z. N. Bao, *Adv. Mater.* **2012**, *24*, 3223; d) S. Jung, J. H. Kim, J. Kim, S. Choi, J. Lee, I. Park, T. Hyeon, D. H. Kim, *Adv. Mater.* **2014**, *26*, 4825; e) S. Park, H. Kim, M. Vosgueritchian, S. Cheon, H. Kim, J. H. Koo, T. R. Kim, S. Lee, G. Schwartz, H. Chang, Z. Bao, *Adv. Mater.* **2014**, *26*, 3451; f) J. Park, Y. Lee, J. Hong, Y. Lee, M. Ha, Y. Jung, H. Lim, S. Y. Kim, H. Ko, *ACS Nano* **2014**, *8*, 12020.
- [7] T. Sekitani, T. Someya, *MRS Bull.* **2012**, *37*, 236.
- [8] W. Luheng, D. Tianhuai, W. Peng, *Sens. Actuators A* **2007**, *135*, 587.
- [9] D. J. Lipomi, M. Vosgueritchian, B. C. Tee, S. L. Hellstrom, J. A. Lee, C. H. Fox, Z. Bao, *Nat. Nanotechnol.* **2011**, *6*, 788.
- [10] X. Wang, Y. Gu, Z. Xiong, Z. Cui, T. Zhang, *Adv. Mater.* **2014**, *26*, 1336.